Effect of Occluded Ligand Migration on Kinetics and Structural Dynamics of Homodimeric Hemoglobin

Hanui Kim,[†,‡,Δ] Jong Goo Kim,[†,‡,Δ] Srinivasan Muniyappan,[†,‡,§,Δ] Tae Wu Kim,[†,‡,#] Sang Jin Lee,[†,‡] and Hyotcherl Ihee[,†,‡]*

† Department of Chemistry and KI for the BioCentury, KAIST, Daejeon 305-701, Republic of Korea

‡ Center for Nanomaterials and Chemical Reactions, Institute for Basic Science (IBS), Daejeon 305-701, Republic of Korea

§ Present address: Department of New Biology, Daegu Gyeongbuk Institute of Science and Technology, Daegu 42988, Republic of Korea

Present address: Chemical Sciences and Engineering Division, Argonne National Laboratory, Lemont, Illinois 60439, United States

* Corresponding Author: hyotcherl.ihee@kaist.ac.kr

Δ H.K., J.G.K., and S.M. contributed equally to this work.

- Table of Contents -

1. Sample preparation

The I114F mutation (I114F) was introduced into the native recombinant HbI gene using the Exchange® mutagenesis kit (Enzynomics[TM]) with the following primers encoding I114F mutation: 5'-gaattcggtaaattcaacggtccgatc-3' and 5'-gatcggaccgttgaatttaccgaattc-3'. I114F was over-expressed and purified as described for the wild type (WT),[1] Carbonmonoxy derivatives of I114F solution for the photodissociation reaction were prepared as follows. A 2-4 mM deoxy I114F solution in 100 mM of a phosphate buffer (pH 7) was prepared in a rubber-topped air-tight vial. The concentration of the protein solution was determined from the absorbance at 578 nm using the extinction coefficient of heme-oxygenated derivatives (14.3 $mM^{-1}cm^{-1}$). The deoxy I114F was reduced by adding 10 μl of a 1M sodium dithionite solution under a nitrogen atmosphere. To convert deoxy to the CO-bound I114F, the reduced samples were exposed to CO gas for 30 min. The sample solution was prepared just before the X-ray solution scattering measurement. An aliquot of the resulting I114F $HbI(CO)_2$ solution was transferred into a quartz capillary with a diameter of 1 mm (Hampton Research) and immediately sealed.

2. Data collection

Time-resolved X-ray solution scattering data of I114F in the solution were collected at the 14IDB beamline at the Advanced Photon Source (APS) based on the pump-probe method. First, the solution sample of CO-ligated I114F HbI sealed in a capillary with a 3.5 mM concentration was excited by a laser pulse. For the pump pulse to excite the sample, we used circularly polarized laser pulses with a duration of ~35 ps and a center wavelength of 532 nm at a focal spot of 0.15 x 0.60 mm^2 with fluence of 1.0 mJ/mm^2. The pump pulse was focused on the top of the capillary. To monitor the photo-induced structural changes of the sample, a subsequent X-ray pulse was

delivered with a time delay, Δt. The X-ray pulses with 10^9 photons had an energy spectrum which peaked at 12 keV with a bandwidth of 4% and were focused to a size of 0.09 x 0.07 mm^2. The X-ray pulse probes 0.2 mm deep from the top in perpendicular geometry. To provide a fresh sample for every exposure of the pump and probe pulses, the sealed capillary was translated back and forth along its long axis. The temperature of sample was maintained at 298 K with a nitrogen stream (Oxford Cryostream). X-ray scattering images were collected using an area detector (Rayonix) for 36 pump-probe time delays in the range of 100 ps to 56.2 ms (four time points per decade).

3. Data processing

Two-dimensional X-ray scattering patterns are centrosymmetric due to the random orientation of the molecules in the solution. We azimuthally integrated the two-dimensional X-ray scattering image and obtained one-dimensional scattering curves as a function of the magnitude of the momentum transfer vector, $q = (4\pi/\lambda)\sin(2\theta/2)$. To convert the scattering angle (2θ) to the momentum transfer vector (q), the center-of-mass position of the undulator spectrum was used as the reference wavelength (λ).

Since a majority of scattering signal comes from solvent pairs or bulk solvent, the laser-induced scattering intensity changes are less than a few percent of the static scattering intensity. To extract the underlying scattering signal from solute molecules, we obtained time-resolved difference X-ray solution scattering curves at the time delay of t, $\Delta S(q, t)$, shown in Figure S1 after careful normalization. As a normalization reference, we used a q position of 2.07 Å^{-1}, which is the isosbestic point of the water scattering curves with respect to the temperature, so that the difference scattering intensity at this q value is zero.

The scattering contribution arising from the solvent heating in the time-resolved difference X-ray solution scattering curves was removed by the following procedures. In Figure S3, the difference curves at 31.6 ms and 56.2 ms are shown as examples confirming that the difference scattering at late time delays are mainly attributed to solvent heating. The difference scattering curves are similar to the scattering curve arising from the water thermal heating, indicating that the contribution from transiently generated species is negligible. In addition, the signal where $q >$ 1.0 Å^{-1} can be represented by a thermal heating signal of bulk water, which is represented by a sum of the temperature change at constant density $((\partial S(q)/\partial T)_\rho)$ and the density change at constant temperature $((\partial S(q)/\partial\rho)_T)$. This fitted curve, represented by a linear combination of $((\partial S(q)/\partial T)_\rho)$ and $((\partial S(q)/\partial\rho)_T)$, was subtracted from the difference curves at all time delays to remove the solvent heating effect (see Figure S2).

4. SVD analysis

The time-resolved difference X-ray solution scattering curves, $\Delta S(q,\ t)$, following photolysis of the ligand for I114F in the solution, are shown in Figure 2. The time-resolved difference scattering curve at each time delay shows the oscillatory feature attributed to the intermediates existing in that time delay. Thus, time-resolved difference scattering curves are composed of the intrinsic difference scattering curves of the intermediates, termed the species-associated difference scattering (SADS) curve, and the population changes of the intermediates over time. These two components can be extracted by a kinetic analysis. As the first step of the kinetic analysis, we conducted a singular value decomposition (SVD) analysis of the TRXSS data, which provided information about the number of structurally identifiable intermediates present in the total time range of the TRXSS data and their transition time constants. To perform the SVD

analysis on the TRXSS data, the entire dataset is represented as a matrix, whose column is the difference scattering curve of each time delay. When we applied SVD to the matrix, the matrix is decomposed with left singular vectors (lSVs, U), right singular vectors (rSVs, V), and singular values (s, S), corresponding to the basis for spanning by the SADS curves of the intermediates, the basis of the time-dependent concentration changes of the intermediates, and the contribution of the basis, respectively. The number of structurally distinct intermediates can be determined by the number of singular vectors having significant singular values. In addition, as the amplitude changes of rSVs arise due to linear combinations of the time-dependent concentration changes of the intermediates, the global fitting of rSVs with the sum of the exponential functions indicate the rates of the transition between the intermediates. When we applied the SVD analysis to the TRXSS data of I114F in a q-range of 0.15 Å^{-1} to 1.0 Å^{-1}, there exist three significant components, as shown in Figure S4, indicating that the I114F HbI(CO)$_2$ in the solution underwent a photoreaction through three structurally distinct intermediates. As shown in Figure S4d, the first three rSVs of I114F are multiplied by singular values and then are fitted with the sum of six exponentials with time constants of 640 ($\pm$ 96) ps, 23 ($\pm$ 1.5) ns, 990 ($\pm$ 190) ns, 7.6 ($\pm$ 1.0) μs, 3.2 ($\pm$ 0.41) ms, and 29 ($\pm$ 24) ms. The numbers of time constants differ in WT and I114F, at seven and six, respectively.

5. Kinetic model

From the SVD analysis, we found that the number of intermediates in I114F is identical to that in WT, but with six time constants, one less than that of WT. Therefore, it was necessary to construct a new kinetic model for I114F because it is difficult to apply the kinetic model for WT to the TRXSS data of I114F. Because the recovery of the ground state $HbI(CO)_2$ from I_3 is bimolecular kinetics in I114F, as well as in WT, the last two time constants of the mutant (3.2 ms and 29 ms) were used to approximate the rate constant for the bimolecular CO recombination.

To identify the dynamics of I_1, I_2, I_3 and $HbI(CO)_2$ with the four remaining time constants, we applied an SVD analysis in a reduced time range, which provides the number of intermediates existing in that time range. Figures S5a, S5b, and S5c show the first three lSVs obtained by the SVD analysis in the time range from 100 ps to the time delay containing the first, second, and third time constant, respectively. We observed that one, two, and three lSVs have clear oscillatory feature in Figures S5a, S5b, and S5c, respectively. This means that there exist one, two and three intermediates in each time range. In Figure S5a, because only one component exists in the time range from 100 ps to 1 ns, covering the first time constant, the time constant of 640 ps explains not the I_1-to-I_2 transition but the geminate recombination of I_1 forming the initial state. In Figure S5b, given that the second intermediate appears in the time range from 100 ps to 31.6 ns, I_1 transforms to I_2 with the second time constant of 23 ns. In Figure S5c, the third component becomes dominant in the time range from 100 ps to 980 μs, indicating that I_3 is formed with a time constant of 990 ns. Therefore, based on the SVD analyses with the various time ranges, we could suggest the kinetics of I114F, which consists of a geminate recombination of I_1, an I_1-to-I_2 transition, and an I_2-to-I_3 transition with corresponding time constants of 640 ps, 23 ns, and 990 ns, respectively.

The remaining time constant, 7.6 μs, was assigned to the slower time constant of the biphasic transition from I_2 to I_3. Similar to the kinetic model for WT, we interpreted that the fast and slow time constants (990 ns and 7.6 μs) of the biphasic kinetics correspond to the R-T transitions of the fully photolyzed form and the partially photolyzed form, respectively. In our study on WT,[2] the branching ratio between the two time constants of biphasic I_2-to-I_3 transitions exhibits the dependence on the excitation laser fluence and the similar dependency was observed in a transient absorption experiment as well.[3] In detail, we related the fast and slow components to the fully and partially photolyzed forms of intermediate I_2, respectively, based on the fact that.the ratio of the fast component with respect to the slow component decrease as the fluence of the pump pulse decreases.

6. Kinetic analysis

In the kinetic analysis, the theoretical difference scattering curve at each time delay is generated by a linear combination of the first three lSVs based on the kinetics model. The time evolution of the theoretical time-resolved difference scattering curves is described by the concentration changes of the intermediates, expressed by a set of kinetic parameters, 1) the ratio of the geminate and non-geminate recombination, 2) the ratio between fully and partially photolyzed forms, and 3) the rate for nongeminate recombination. Minimizing the discrepancy between the theoretical and experimental difference scattering curves at all time delays (quantified by the chi2 value) allows us to optimize the kinetic parameters. Only when the suggested kinetic model describes the kinetics involved in the TRXSS data, sufficient agreement between the theoretical and experimental scattering curves at all the time delays can be achieved. As a result of the kinetics analysis, we could determine the optimum kinetic parameters (Table S1) and extract

the time-dependent concentration changes (Figure 3c) and time-independent SADS curves (Figure 3d) of the three intermediates.

We noted that the ratio between the geminate and non-geminate recombination was determined from the kinetic analysis by using the fraction of geminate recombination as a free parameter. The fraction of geminate recombination was determined to be 16 %, indicating that 16 % of I_1 returns to the initial I114F $HbI(CO)_2$ by the geminate recombination with a time constant of 640 ps. The rest of I_1 transforms into I_2 with a time constant of 23 ns. If the two processes with time constants of 640 ps and 23 ns are in a kinetically competitive relationship, ~97 % of I_1 should return to the initial I114F $HbI(CO)_2$ with a time constant of 640 ps. However, only 16 % of I_1 undergoes the geminate recombination, indicating that those processes are not kinetically controlled. It can be explained by two different substates of I_1, which have two different destinies with respect to the structural change but are indistinguishable by TRXSS. Similarly, a branching ratio between competing reaction pathways, which are not kinetically controlled, was observed in TRXSS study on sperm whale myoglobin.[4] In the study, it was revealed that the transition from the first intermediate to second intermediate occurs biphasically with time constants of 460 ps and 3.6 ns. If the two pathways compete with each other kinetically, the branching ratio between the faster and slower components should be 90 % and 10 %, respectively, considering their time constants, so that most of the population should transit with the faster time constant. However, the actual branching ratio between the faster and slower components were determined to be 46 % and 54 %, respectively, from the kinetic analysis using the ratio as a fitting parameter. This comparable ratio between the faster and slower components indicates that the transition from the first to second intermediates exhibiting the biphasic kinetics is not a kinetically controlled process. To address the discrepancy, we suggested that there might be a predetermined ratio between the two pathways.

One of the possible explanations is the existence of conformational substates in the first intermediate generated by the interplay between the distal histidine and the photodissociated CO, which are not distinguished by TRXSS signal but transit to the subsequent intermediate with different time constants.

7. Origin of the small amplitude in the SADS curve of I114F

In the main text, we mentioned that the difference in the amplitude of the SADS curves between I114F and WT shown in Figure 3d, is attributed to the difference in the magnitude of the structural change between I114F and WT. Since the 2.8 times smaller magnitude in the SADS curve of I_3^{I114F} can also arise when the smaller population of I_3^{I114F} is formed during the photocycle, we examined the possibility that the actual amount of I_3^{I114F} is smaller than that of WT. The population of I_3^{I114F} can be lower when the quantum yield of the photodissociation is smaller in I114F or the fraction of the geminate recombination is larger in I114F. We checked if those two possibilities are plausible considering our TRXSS data and the results of the kinetic analysis.

To check if the quantum yield of the photodissociation is lower in I114F than that in WT, we expected the fraction of the photodissociated molecules for I114F and WT. For this purpose, we checked 1) the absorbance of I114F and WT at 532 nm, 2) the number of photons and protein molecules in the probed volume in both of the TRXSS experiments for I114F and WT, and 3) the quantum yield of the photodissociation of CO from heme proteins. First, the absorbance of I114F and WT are similar at a wavelength of 532 nm under the same concentration and pathlength, as shown in Figure S6. Second, the number of photons is much larger than that of protein molecules in the probed volume in both TRXSS experiments for I114F and WT. We estimated the numbers of photons and protein molecules from the laser fluence and the sample concentration. For I114F,

the laser pulse contains 1.9×10^{14} photons/pulse and the probed volume contains 3.0×10^{13} protein molecules. For WT, the laser pulse contains 7.9×10^{13} photons/pulse and the probed volume contains 1.4×10^{13} protein molecules. As a result, for both I114F and WT, the number of photons is ~6 times larger than the number of protein molecules in the probed volume. More details are described in the section "Photoconversion yield". Third, it is well known that the quantum yields of the photodissociation of CO from heme proteins are almost unity.[5] Considering the three factors described above, we expect that most of the protein molecules were photodissociated in the TRXSS experiments for both I114F and WT. In other words, the quantum yields of the photodissociation of I114F and WT are similar to each other, nearly equal to unity. In addition, if the quantum yield of the photodissociation was lower in I114F than that in WT, the magnitude of the SADS curve of I_1^{I114F} should be also 2.8 times smaller than that of WT, as in the case of I_3^{I114F}. However, as can be seen in Figure S7, the difference in the magnitudes of SADS curves between I114F and WT is less pronounced in I_1, compared to the case of I_3.

We checked whether the fraction of geminate recombination is larger in I114F than that in WT, resulting in smaller population of I_3^{I114F}. However, as discussed in the main text, the fraction of geminate recombination in I114F was determined to be 16 %, which is similar to that in WT (19 %).

Therefore, we conclude that the yield of I_3 is not smaller in I114F compared to that in WT and the difference in the amplitude of I_3 SADS curves between I114F and WT can be attributed to the difference in the magnitude of the structural change.

8. Relation between the amplitude of the SADS curve and the magnitude of the structural change

To inspect the relation between the amplitudes of SADS curves and the magnitude of the structural changes, we performed simple simulations. The three types of the structural changes with three different magnitudes were simulated and the difference scattering curves arising from the structural changes were compared to each other. We compared the difference scattering curves arising from the structural changes when the forces are applied in the same direction but different magnitudes. For this purpose, we induced the structural changes by applying the forces of $\mathbf{F}$, $2\mathbf{F}$ and $3\mathbf{F}$ to crystal structure of I114F (pdb code: 1JZK) in the same direction. The simulated difference scattering curves between crystal structure and the perturbed structure obtained by applying the force of $\mathbf{F}$ (black), $2\mathbf{F}$ (red), and $3\mathbf{F}$ (blue) are compared in Figure S8a. In Figure S8b, the three simulated difference scattering curves obtained by applying $\mathbf{F}$ (black), $2\mathbf{F}$ (red), and $3\mathbf{F}$ (blue) become almost identical to each other when the curves are divided by 1, 2, and 3, respectively. This further confirms that the difference in the amplitude of I_3 SADS curves between WT and I114F can arise from the difference in the magnitude of the structural change.

9. Structure refinement

We performed a structure refinement analysis using the SADS curves of the three intermediates for I114F, as was done for the structures of the intermediates in WT. For the structure refinement analysis, we applied a rigid-body modeling approach where the crystallographic structure was used as a template structure to determine the atomic-level structure of an intermediate. The entire protein structure was divided into eighteen rigid bodies, that is, eight helices and a heme group for each subunit. The positions and orientations of the rigid bodies were changed based on a Monte Carlo simulation algorithm to minimize the discrepancy between the theoretical difference scattering curve calculated from the refined structure and the SADS curve obtained

from the experiment. To avoid being trapped in local energy minima, we generated many initial structures for the structure refinement process by randomly moving the rigid bodies from a known crystal structure rather than using only one crystal structure. For each intermediate, we repeated the refinement process for 480 different initial structures whose rigid bodies are randomly displaced from the template structure. We used liganded crystal structure of I114F (pdb code: 1JWN) as the reference structure, that is, the initial I114F $HbI(CO)_2$, and unliganded crystal structure of I114F (pdb code: 1JZK) as the template structure for the three intermediates of the mutant.[6] We modified the unliganded crystal structure of I114F to be the template structure of each intermediate. For the I_1 and I_2 intermediates, the ligand resides in the protein and the number of subunit interface water molecules is 12, corresponding to that of allosteric T-state known from the time-resolved X-ray crystallography. In the I_3 intermediate, the ligand is out of the protein and 17 ordered water molecules are at the subunit interface. From the refinement of the initial structures, we selected candidate structures that exhibit a quantified value of the discrepancy between the experimental and theoretical difference scattering curves below a certain threshold. As a result, we obtained 112, 106, and 51 candidate structures for the I_1, I_2, and I_3 intermediates, respectively. The theoretical difference scattering curves for the refined candidate structures are shown in Figure S9.

10. Photoconversion yield

The focal spot of the laser pulse was elliptical with 0.15 x 0.6 mm^2 dimensions with an energy density 1 mJ/mm^2 at 532 nm, giving 1.9×10^{14} photons/pulse. In the interaction volume of 1.4×10^{-5} cm^3, 3.0×10^{13} protein molecules are contained, which is 6.4 times smaller than the number of photons in the laser pulse. Since the extinction coefficient is very high (14.1 mM^{-1}cm^{-1}) at 532 nm, the optical density is 0.99 for the 0.2 mm penetration depth and the 3.5 mM sample solution concentration. As a result, it turned out that the experimental condition regarding the fluence of the pump laser was enough to excite all the protein molecules. Moreover, it is well known that the quantum yield of the photodissociation of CO from a heme protein is almost unity,[5] and thus we expect that 100 % conversion of the initial I114F HbI(CO)$_2$ to the earliest intermediate, I$_1$, in interaction volume was achieved under our experimental conditions. In the same way, 100 % photoconversion is expected to have been achieved in our previous WT experiment (energy density of laser pulse at 532 nm: 0.5 mJ/mm^2, sample concentration: 2.0 mM). Therefore, we compared the kinetics and structural dynamics between I114F and WT, which are obtained based on the fact that 100 % photoconversion yield is achieved both for I114F and WT.

Even in the worst case, for example if the photodissociation is 50 % in reality but we still use 100%, the effect will be as follows. When the photodissociation is 50 %, the kinetic parameters such as time constants, the rate constant for nongeminate recombination, the fraction of geminate recombination, and the ratio between fully and partially photolyzed forms are not affected. The only affected result is the SADS curves, whose amplitudes are twice larger than the case that the 100 % photoconversion occurs. If we refine the structures of intermediates using SADS curves with the enlarged amplitude, the resulting amount of structural change between the intermediates and the ground state is larger than that obtained with 100 % photoconversion. To confirm the

relationship between the magnitude of a difference scattering curve and the amount of structural change, we compared the difference scattering curves arising from the structural changes when the forces are applied in the same direction but different magnitude (see 'Relation between the amplitude of the SADS curve and the magnitude of the structural change' in the SI). The result confirms that the difference in amplitude of SADS curves caused by photoconversion yield can lead to the difference in magnitude of structural change. Therefore, if our assumption of 100 % photoconversion is wrong, the structural parameters would be underestimated compared with the true ones, but the discussion about the direction of structural change would not be affected. Moreover, the photoconversion yield would not affect the discussion about the relative comparison with WT because any wrong estimation of the photoconversion yield would apply to both I114F and WT.

11. Table and Figures

Table S1. Kinetic parameters obtained from kinetic analysis of TRXSS data of I114F.

Parameters	Fit value
Time constant for geminate recombination	640 ($\pm$96) ps
Time constant for I_1-to-I_2 transition	23 ($\pm$1.5) ns
Faster time constant for R-T transition	990 ($\pm$190) ns
Slower time constant for R-T transition	7.6 ($\pm$1.0) us
Rate constant for bimolecular CO recombination	47 ($\pm$0.3) mM^{-1}s^{-1}
Fraction of geminate recombination	16 ($\pm$0.4) %
Fraction of fully photolyzed forms	53 ($\pm$0.4) %
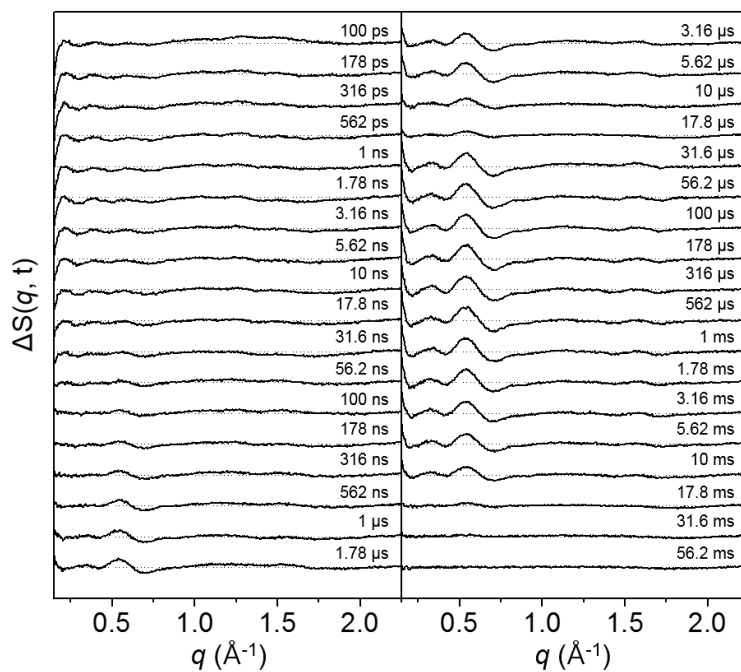
Figure S1. Time-resolved difference X-ray solution scattering curves of I114F. We used q position of 2.07 Å^{-1} as a normalization reference, so that the difference scattering intensity at this q point is zero.
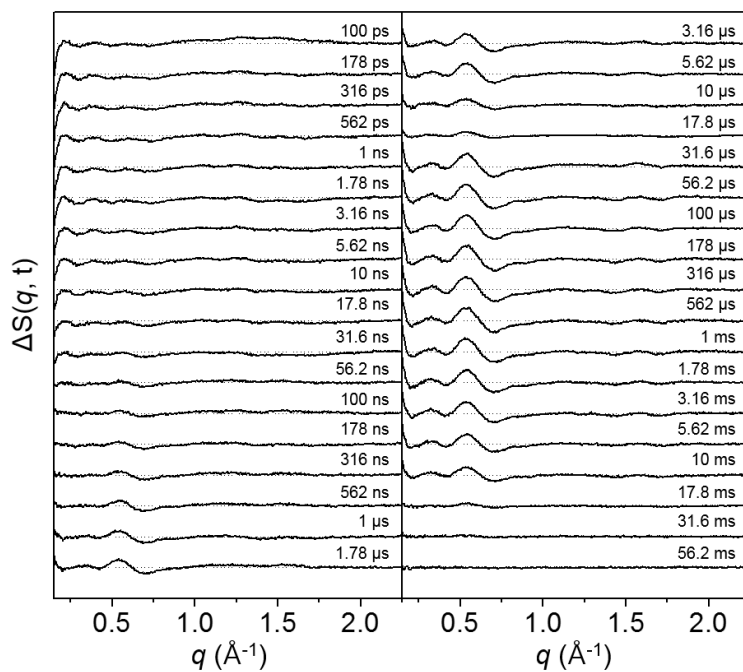
Figure S2. Heat-free, time-resolved difference X-ray solution scattering data of I114F. Thermal heating signal of bulk water shown in Figure S3 was subtracted from the original difference curves shown in Figure S1.
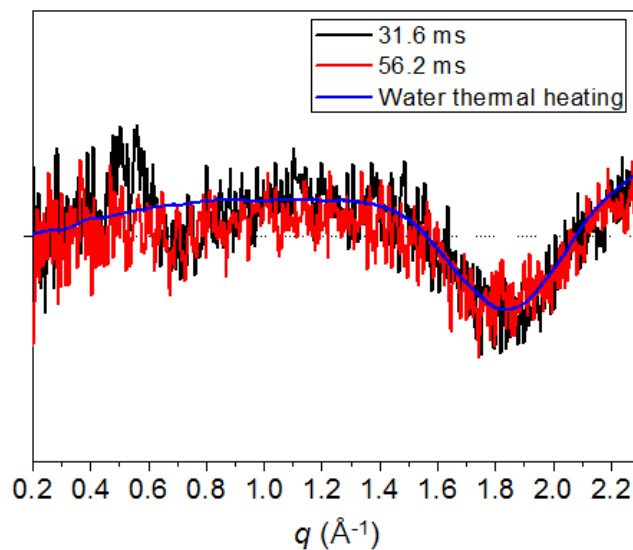
Figure S3. The difference solution scattering curves at 31.6 ms (black) and 56.2 ms (red) time delays and water thermal heating signal (blue). At these time delays, the difference scattering curves are similar to the scattering curve arising from the water thermal heating, indicating that the contribution from transiently generated species is negligible. The signal in the region where q > 1.0 Å^{-1} can be represented by a thermal heating signal of bulk water, which can be represented by a sum of the temperature change at constant density $((\partial S(q)/\partial T)_\rho)$ and the density change at constant temperature $((\partial S(q)/\partial \rho)_T)$. In other words, the difference signals at late time delays are mainly attributed to solvent heating.
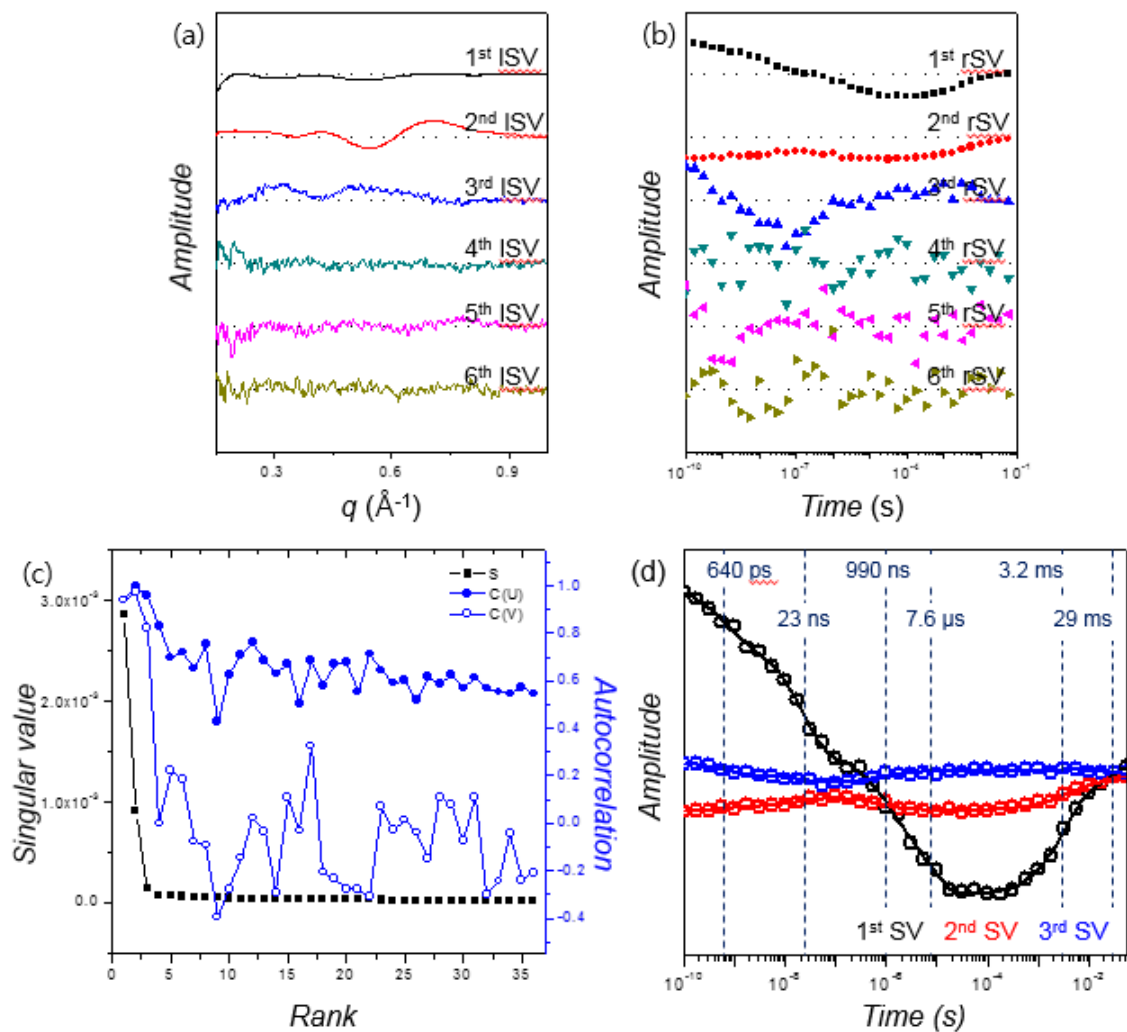
Figure S4. (a) The first six lSVs, (b) The first six rSVs (c) Singular values (S, black solid square), autocorrelations of lSVs (C(U), blue solid circle) and autocorrelations of rSVs (C(V), blue open circle) are shown. (d) The first three rSVs multiplied by singular values were fitted by using six exponentials sharing common time constants, yielding the time constants of 640 ($\pm$ 96) ps, 23 ($\pm$ 1.5) ns, 990 ($\pm$ 185) ns, 7.6 ($\pm$ 1.0) us, 3.2 ($\pm$ 0.41) ms, and 29 ($\pm$ 24) ms were obtained.
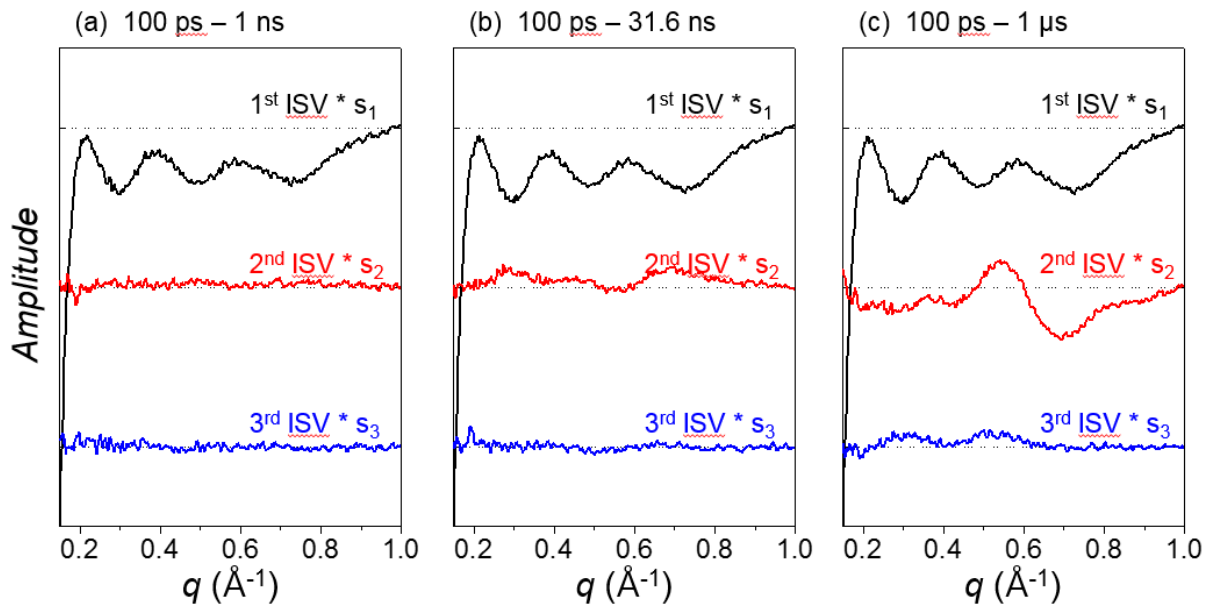
Figure S5. The result of SVD analysis in three different time ranges. (a) The first three lSVs multiplied by singular values in the reduced time range from 100 ps to 1 ns, which contains the first time constant (640 ps) are shown. Only the first lSV has clear oscillatory feature. (b) The first three lSVs multiplied by singular values in the reduced time range from 100 ps to 31.6 ns, which contains the first and second time constant (640 ps and 23 ns), are shown. The first two lSVs have distinct oscillatory features. (c) The first three lSVs multiplied by singular values in reduced time range from 100 ps to 1 μs, which contains the first three time constants (640 ps, 23 ns, and 990 ns), are shown. The three lSVs have distinct oscillatory features.
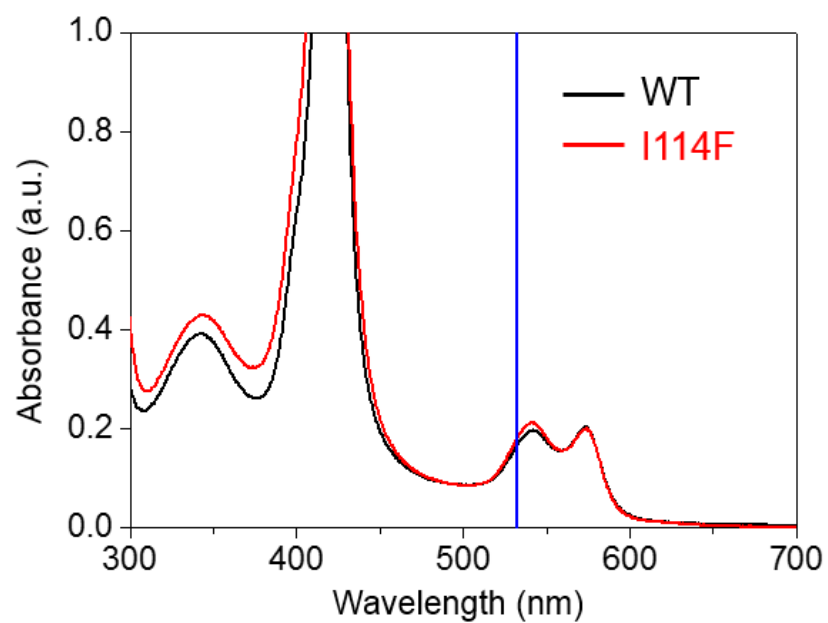
Figure S6. UV-Vis spectrum of WT (black) and I114F (red). The vertical blue line indicates 532 nm. For both WT and I114F, the concentration was 12.6 µM and pathlength was 1 cm.
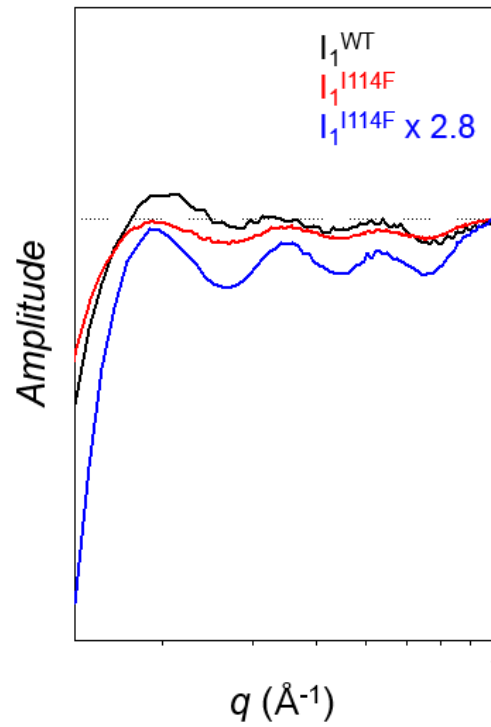
Figure S7. The SADS curves of I_1^{WT} (black) and I_1^{I114F} (red) and scaled SADS curves of I_1^{I114F} (blue). While the magnitude of the SADS curve of I_1^{I114F} is slightly smaller than that of I_1^{WT}, the magnitude of the 2.8-times scaled SADS curve of I_1^{I114F} is considerably larger than that of the SADS curve of I_1^{WT}. This means that the pronounced reduction by 2.8 times observed for I_3^{I114F} is not found in I_1^{I114F}.
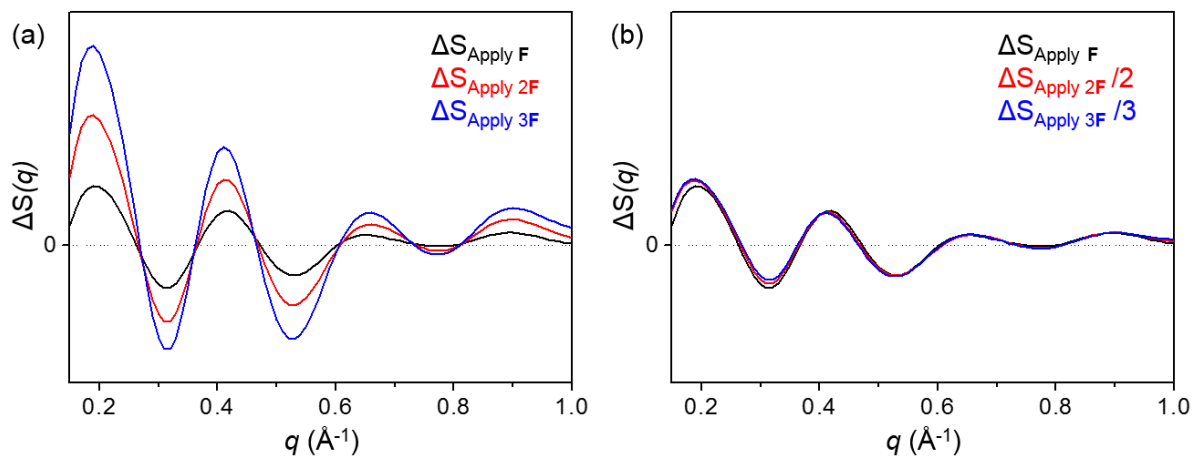
Figure S8. Relationship between the amount of structural change and the magnitude of a difference scattering curve. (a) The simulated difference scattering curves arising from the structural changes by applying **F** (black), 2**F** (red) and 3**F** (blue). (b) The simulated difference scattering curves obtained by applying **F** (black), 2**F** (red) and 3**F** (blue) are divided by 1, 2, and 3, respectively.
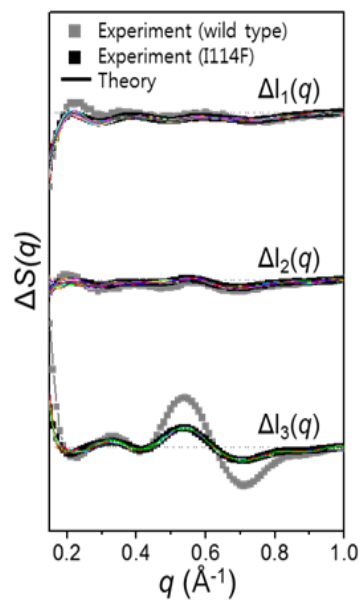
Figure S9. SADS curves of three intermediates of WT (gray dots) and I114F (black dots) and theoretical difference scattering curves calculated from the best fitted structures of I114F (colored lines).
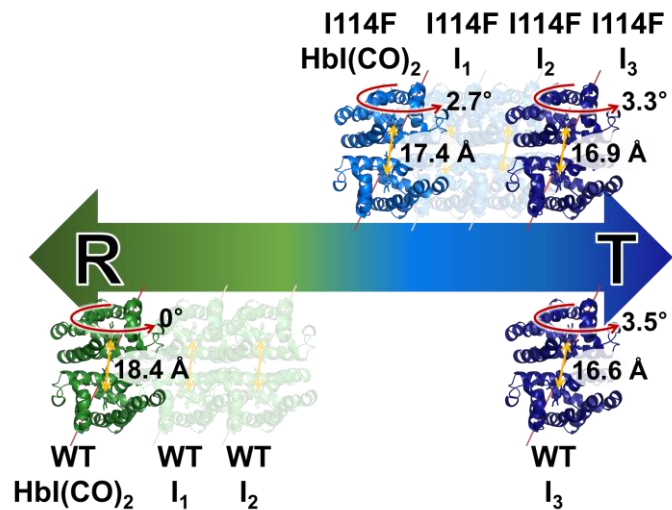
Figure S10. Schematic summary of the structural transition for WT and I114F. In WT, the structures of I_1 and I_2 are close to that of R state of WT and the structure of I_3 is close to that of T state of WT. In I114F, because the starting structure of R-T transition is already shifted toward the T state of WT, all of I_1, I_2, and I_3 have structures close to T state of WT.

12. References

1.   Summerford, C. M.; Pardanani, A.; Betts, A. H.; Poteete, A. R.; Colotti, G.; Royer, W. E., Jr., Bacterial expression of Scapharca dimeric hemoglobin: a simple model system for investigating protein cooperatively. *Protein Eng.* **1995,** *8* (6), 593-9.

2.   Kim, K. H.; Muniyappan, S.; Oang, K. Y.; Kim, J. G.; Nozawa, S.; Sato, T.; Koshihara, S. Y.; Henning, R.; Kosheleva, I.; Ki, H.; Kim, Y.; Kim, T. W.; Kim, J.; Adachi, S.; Ihee, H., Direct Observation of Cooperative Protein Structural Dynamics of Homodimeric Hemoglobin from 100 ps to 10 ms with Pump-Probe X-ray Solution Scattering. *J Am Chem Soc* **2012,** *134* (16), 7001-7008.

3.   Chiancone, E.; Elber, R.; Royer, W. E., Jr.; Regan, R.; Gibson, Q. H., Ligand binding and conformation change in the dimeric hemoglobin of the clam Scapharca inaequivalvis. *J. Biol. Chem.* **1993,** *268* (8), 5711-5718.

4.   Oang, K. Y.; Kim, J. G.; Yang, C.; Kim, T. W.; Kim, Y.; Kim, K. H.; Kim, J.; Ihee, H., Conformational Substates of Myoglobin Intermediate Resolved by Picosecond X-ray Solution Scattering. *J. Phys. Chem. Lett.* **2014,** *5* (5), 804-808.

5.   Noble, R. W.; Brunori, M.; Wyman, J.; Antonini, E., Studies on the quantum yields of the photodissociation of carbon monoxide from hemoglobin and myoglobin. *Biochemistry* **1967,** *6* (4), 1216-1222.

6.   Knapp, J. E.; Gibson, Q. H.; Cushing, L.; Royer, W. E., Jr., Restricting the ligand-linked heme movement in Scapharca dimeric hemoglobin reveals tight coupling between distal and proximal contributions to cooperativity. *Biochemistry* **2001,** *40* (49), 14795-14805.